American Mineralogist, Volume 92, pages 344–355, 2007

# Elastic anomalies accompanying phase transitions in (Ca,Sr)$TiO_3$ perovskites: Part III. Experimental investigation of polycrystalline samples

MICHAEL A. CARPENTER,[1,*] BAOSHENG LI,[2] AND ROBERT C. LIEBERMANN[2]

[1]Department of Earth Sciences, University of Cambridge, Downing Street, Cambridge CB2 3EQ, U.K.
[2]Department of Geosciences, SUNY at Stony Brook, Stony Brook, New York 11794, U.S.A.

## ABSTRACT

Bulk and shear moduli of polycrystalline samples of perovskites with different compositions across the $CaTiO_3$-$SrTiO_3$ solid solution have been measured at ambient conditions and in-situ at high pressures by pulse-echo ultrasonic methods. The samples were prepared as dense pellets by hot pressing synthetic powders at ~7.5 GPa and ~1000 °C. Any variations of bulk modulus due to phase transitions are small, but significant anomalies have been observed in the shear modulus at ambient conditions. These are associated with a sequence of symmetry changes $Pm\bar{3}m \rightarrow I4/mcm \rightarrow Pbcm \rightarrow Pnma$ with increasing $CaTiO_3$ content. Comparison with variations in elastic properties predicted using Landau theory suggests that a substantial part of the elastic softening observed in tetragonal samples could be due to anelastic contributions from transformation twin walls. This additional softening does not occur in orthorhombic samples, and the transition from tetragonal to orthorhombic symmetry results in a stiffening of the shear modulus. No overt evidence was found for a phase transition $I4/mcm \leftrightarrow Pnma$ at high pressures in $Ca_{0.35}Sr_{0.65}TiO_3$ but small changes in the trends of both bulk and shear moduli in the range 2.5–3 GPa could be due either to a different transition or a change in compression mechanism. A $Pm\bar{3}m \leftrightarrow I4/mcm$ transition at ~2 GPa in $Ca_{0.05}Sr_{0.95}TiO_3$ shows the same form of softening as observed for the transition as a function of composition. A simple model of twin wall contributions to the compliance of tetragonal samples failed to match the observed variations that, alternatively, seem to follow $\Delta G \propto q_4$ where $\Delta G$ is the change in shear modulus and $q_4$ the driving order parameter for the $Pm\bar{3}m \leftrightarrow I4/mcm$ transition. Analogous elastic behavior is expected to occur in (Mg,Fe)$SiO_3$ and $CaSiO_3$ perovskites at high pressures and temperatures.

**Keywords:** Elastic constants, phase transitions, $CaTiO_3$-$SrTiO_3$ solid solution, anelasticity

## INTRODUCTION

A prerequisite for experimental determinations of the complete set of elastic constants for a mineral is usually the availability of suitable single crystals. An alternative approach is to work with polycrystalline aggregates in the form of a ceramic, however. Powder of the sample of interest is hot pressed to give a mechanically robust, low porosity, dense pellet. The pellet is then polished and conventional methods, such as pulse-echo ultrasonics, are used to measure the velocities of P and S waves propagated through it. Only the bulk ($K$) and shear ($G$) moduli are obtained from such samples, but these are usually the elastic properties of most immediate interest in a geophysics context. This approach was pioneered for elastic measurements on perovskites at ambient conditions and in-situ at high pressures by Liebermann et al. (1977). It has subsequently been used to measure the bulk elastic properties of a variety of synthetic perovskites (Fischer et al. 1989, 1993; Sinelnikov et al. 1998a, 1998b; Kung and Rigden 1999; Kung et al. 2000a, 2001). The use of ceramic samples and pulse-echo methods has also been used for in-situ measurements at high temperatures (Webb et al. 1999; Kung et al. 2000b) and to follow elasticity variations across a binary perovskite solid solution (Sinelnikov et al. 1998a). In-situ measurements at simultaneous high temperatures and pressures are also possible (Sinelnikov et al. 1998b; Li et al. 2004). The present study was designed in the light of these successes, with the specific objective of characterizing anomalies in elastic properties that are due to cubic ($Pm\bar{3}m$) ↔ tetragonal ($I4/mcm$) and tetragonal ($I4/mcm$) ↔ orthorhombic ($Pnma$) transitions in perovskites with compositions across the $CaTiO_3$-$SrTiO_3$ (CST) solid solution.

The CST system displays phase transitions that appear to be closely analogous to transitions that might occur at high pressures and temperatures in (Mg,Fe)$SiO_3$ and $CaSiO_3$ perovskites. The transitions occur at pressures and temperatures that are amenable to direct observation, and the form of the elastic anomalies can be predicted using Landau theory. The present paper is the third in a sequence on this subject. In the first paper (Carpenter 2007a), a fully parameterized Landau model was presented for the $Pm\bar{3}m \leftrightarrow I4/mcm$ transition in $SrTiO_3$. In the second paper (Carpenter 2007b), the model was extended to describe the influence of composition across the CST solid solution. Both papers contain equations that predict elastic behavior of the form illustrated in Figure 1 for composition, temperature and pressure as the external variables. Quantitative predictions are tested here against

* E-mail: mc43@esc.cam.ac.uk

0003-004X/07/0203–344$05.00/DOI: 10.2138/am.2007.2297 

new pulse-echo ultrasonic data obtained from samples with different composition across the solid solution at ambient conditions and in-situ at high pressures for samples with compositions $Ca_{0.35}Sr_{0.65}TiO_3$ (CST65) and $Ca_{0.05}Sr_{0.95}TiO_3$ (CST95). Deviations from model behavior are considered in terms of the possible role of twin walls in reducing the effective shear elastic constant, and the form of the real shear modulus variations might be better represented by the dot-dash line in Figure 1. In combination, the theoretical and experimental approaches to the CST perovskite system suggest new insights into the likely elastic behavior of silicate perovskites in the earth's mantle.

Experimental values of *K* and *G* presented below for polycrystalline $CaTiO_3$ and $SrTiO_3$ at ambient conditions are in general agreement with previous data from Bell and Rupprecht (1963), Beattie and Samara (1971), Liebermann et al. (1977), Ishidate et al. (1988), Ledbetter et al. (1990), Fischer et al. (1993), Sinelnikov et al. (1998a), Kung and Rigden (1999), Lheureux et al. (1999), Ross and Angel (1999), and Webb et al. (1999). The only previous study of elastic constants across the CST solid solution appears to be that of Harrison et al. (2003), who followed relative changes of Young's modulus as a function of temperature at 1–320 Hz by Dynamical Mechanical Analysis. The present study is complementary to this in providing absolute values of bulk and shear moduli, measured at tens of MHz. In-situ determinations of the elastic properties of CST perovskites at high pressures appear to be restricted to single-crystal or polycrystalline samples of $CaTiO_3$ (Liebermann et al. 1977; Fischer et al. 1993; Kung and Rigden 1999; Ross and Angel 1999) and $SrTiO_3$ (Edwards and Lynch 1970; Beattie and Samara 1971; Fischer et al. 1989, 1993; Ishidate et al. 1988; Lheureux et al. 1999). There are a few single-crystal X-ray diffraction datasets for CST65 at high pressures (Yamanaka et al. 2002), which suggest that the stable structure at $P \geq 3.5$ GPa has *Pnma* symmetry.

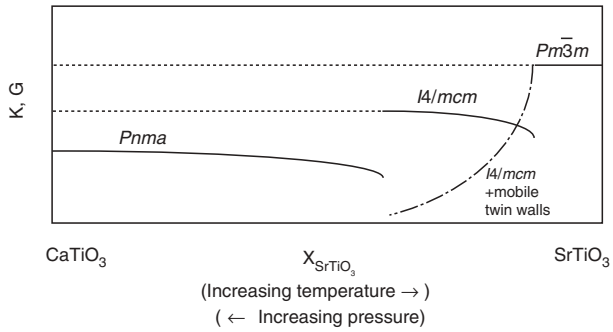


**FIGURE 1.** Schematic representation of relative changes in bulk modulus and shear modulus through the sequence of transitions $Pm\bar{3}m \leftrightarrow I4/mcm \leftrightarrow Pnma$ in CST perovskites (ignoring the *Pbcm* structure that becomes stable at relatively low temperatures). On the basis of Landau expansions presented elsewhere (Carpenter 2007a, 2007b) and excluding the effects of microstructure, each transition is predicted to give rise to discontinuous softening of both *K* and *G* with falling symmetry (solid lines). The amount of curvature just below the transition point depends on how close the evolution of the equilibrium order parameter is to tricritical. Increasing temperature should give a sequence that is analogous to increasing $SrTiO_3$ content, while increasing pressure should give a sequence analogous to increasing $CaTiO_3$ content. The dot-dash line represents an alternative form of elastic softening for the shear modulus of a polycrystalline tetragonal sample in which additional softening contributions are due to the mobility of transformation twin walls.

## EXPERIMENTAL METHODS

### Sample preparation

Samples with 16 different compositions across the CST solid solution were synthesized using a similar method to that used by Ball et al. (1998). Sr-nitrate and Ca-nitrate were dissolved in water. Ti isopropoxide was added to the solution, inducing the formation of a gel-like mixture which was mechanically stirred and then dried at ~120 °C. The dry product was ground in an agate ball mill, calcined at 1050 °C for 12 hours and then ball milled again. Approximately 30 g of intimately mixed fine-grained oxides was prepared for each composition by this method. Three firing cycles were then applied, with mechanical grinding in the agate ball mill between each. The first firing was for 36 hours at 1350 °C, the second for 12 hours at 1600 °C, and the third for 36 hours at 1600 °C, leaving fine-grained powders with a pale cream color. The final products were ball milled at a slower speed than in the intermediate grinding stages (300 rpm rather than 600 rpm), to minimize damage to the crystallites.

Peaks in powder X-ray diffraction patterns collected from the synthetic products could all be indexed as being due to CST perovskite, apart from a barely detectable peak corresponding to a d-spacing of ~3.23 Å, which may indicate the presence of trace amounts of rutile in some samples. The composition of the sample which gave the strongest rutile peak (CST65) was checked by electron microprobe analysis. A piece of the fired sample and the hot pressed pellet were found to contain exactly the expected Ca:Sr ratio and a small excess of Ti. The yield of Ti from the Ti isopropoxide was presumably slightly variable.

The space groups of the present set of samples were assumed to be *Pnma* for CST0–CST55, *Pbcm* for CST60, *I*4/*mcm* for CST65–CST90, and $Pm\bar{3}m$ for CST95 and CST100. This assignment follows Ball et al. (1998) and Qin et al. (2000), who used X-ray powder diffraction for many compositions across the solid solution, Howard et al. (2001) and Ranjan et al. (2001), who used electron diffraction to show that CST50 at room temperature has *Pnma* symmetry, and Yamanaka et al. (2002), who used single-crystal X-ray diffraction to show that the Ca-rich limit of *I*4/*mcm* structures occurs between CST60 and CST65 at room temperature. Mishra et al. (2005, 2006a, 2006b) proposed that CST60 has *Pbcm* symmetry at room temperature, and it has been assumed that this is the space group of the present sample with the same composition. On the basis of Raman evidence presented by Ranson et al. (2005), Mishra et al. also claimed that samples in the range CST65–CST94 have *Imma* symmetry at room temperature, while Woodward et al. (2006) have proposed monoclinic space groups for a range of intermediate compositions. Nevertheless, synchrotron X-ray powder diffraction data support tetragonal lattice geometry for CST70 (Howard et al. 2005) while single-crystal X-ray diffraction data of Yamanaka et al. (2002) for CST65 are consistent with *I*4/*mcm*. Note, however, that the CST65 sample of Yamanaka et al. (2002) actually has pseudocubic lattice parameters, which are closer to those of the *Pbcm* structure than the *I*4/*mcm* structure reported by others.

### Hot pressing

Dense cylindrical pellets of CST, with diameters of ~3 mm, were prepared for acoustic velocity measurements by hot pressing the pale cream powders, following the general methodology described in detail by Gwanmesia and Liebermann (1992), Gwanmesia et al. (1993), and Sinelnikov et al. (1998a). Approximately 0.1 g of each powder was sealed in a cylindrical gold or platinum capsule (or a gold capsule with platinum lid) and pressurized to 7.5 GPa at room temperature in a 2000 ton uniaxial split sphere apparatus (USSA-2000). Temperature was then increased to 1000 °C. After 2 hours, temperature was reduced to 500 °C at constant pressure, over a period of ~30 minutes, before allowing a long slow decompression over a period of up to 15 hours. The sample was then allowed to cool from 500 °C. Some pellets emerged from the metal encasement with small penetrative cracks, which may have developed during depressurization. Hot pressing runs were repeated until samples without cracks were obtained. Each pellet produced in this way was black. Webb et al. (1999) observed the same change in color, from cream to black, in dense pellets of $CaTiO_3$ and $SrTiO_3$ after hot pressing at 0.3 GPa and 1300 °C. Their samples were encased in Fe-metal jackets and they ascribed the change to the reduction of a small percentage of $Ti^{4+}$ to $Ti^{3+}$.

One of the dense pellets produced in an early run (composition CST90) was prepared as a thin foil for transmission electron microscopy. Examination in a 100 kV TEM revealed that the average grain size was around 4 μm. As all the

samples were prepared by essentially the same procedure, it is assumed that this is representative of all the pellets from which elasticity data were obtained. Webb et al. (1999) showed that hot-pressed $CaTiO_3$ grains contain abundant twinning. Similar twinning is likely to have been present in all the orthorhombic and tetragonal CST samples prepared in the present study. Another dense pellet was ground up for powder X-ray diffraction; the diffraction trace confirmed that, within standard limits of resolution, only CST perovskite was present.

All the dense pellets without obvious penetrative cracks were doubly polished for ultrasonic measurements. At this stage their densities were measured by the Archimedes method using distilled water as the weighing fluid. The measured densities were all within ~1% of theoretical densities calculated using published lattice parameter data. Each polished pellet was also mounted in an X-ray diffractometer equipped with an INEL CPS120 position sensitive detector, to collect powder diffraction patterns. All the patterns obtained were again consistent with the pellets being composed only of CST perovskite.

### Ultrasonic measurements at ambient conditions

Travel times of compressional and shear waves through all the dense CST pellets were measured using pulse-echo methods described in detail elsewhere (Li et al. 2002; Sondergeld et al. 2006). P-wave data were collected over a frequency range of 20–70 MHz using a 40 MHz pure compressional mode $LiNbO_3$ transducer. S-wave data were collected in the same way using a 40 MHz pure shear mode transducer. A 0.3 μm thick layer of semi-liquid GPA (1:1 mixture of glycerol and phthalic anhydride) was used as the bonding medium for connecting the sample to the buffer rod. Corrections for the effect of this bonding material were made following the procedure described by Niesler and Jackson (1989). Pulse-echo measurements were simulated offline using carrier frequencies of 40–60 MHz and sinebursts of 6-cycle duration. Travel times were converted to velocities and then to values of bulk and shear moduli using the sample lengths, as measured to ±0.001 mm using a hand held micrometer, and experimentally determined densities.

### Ultrasonic measurements in-situ at high pressures

Hot pressed pellets of CST65 and CST95 were used for measurements of their bulk and shear moduli in-situ at high pressures. The pellets were in the form of cylinders with polished ends (lengths 1.703 and 1.686 mm, respectively), as obtained from hot pressing and subsequent double polishing for ultrasonic measurements at ambient conditions. Each pellet was held in a pyrophyllite octahedron for loading in a modified 1000-ton uniaxial split cylinder apparatus (USCA-1000) of the Kawai type. Details of the assembly of this octahedron are shown in Figure 1 of Sondergeld et al. (2006). Other experimental details of how pressure was applied and measured, as well as how the acoustic waves were generated and transmitted through the samples, are given by Li et al. (1996, 2002), Liebermann and Li (1998), Decremps et al. (2001), Darling et al. (2004), and Sondergeld et al. (2006). A dual mode $LiNbO_3$ transducer (10° Y-cut) was used to generate longitudinal and transverse acoustic signals with unspecified polarization direction for the transverse signal (Kung et al. 2002; Sinelnikov et al. 2004; Li et al. 2004). Pulse-echo overlap measurements were simulated offline, using carrier frequencies of 40–60 MHz and sinebursts of 6-cycle duration. Corrections for the effect of the bonding layer (gold foil) between sample and buffer rod were made using the procedure described by Niesler and Jackson (1989). Calibration of pressure seen by the sample was achieved using observed travel times through the buffer rod and the transition pressures of Bi metal placed near the sample (e.g., see Sondergeld et al. 2006). Measured travel times through each of the CST pellets were converted to acoustic velocities and then to bulk and shear moduli using the room pressure sample lengths and corrections to allow for the effect of increasing pressure based on the method of Cook (1957).

## Experimental results

Experimental data for bulk and shear moduli as a function of composition at room temperature, as obtained in the present study, are listed in Table 1 and illustrated in Figure 2. The new values of *G* for both $CaTiO_3$ and $SrTiO_3$ overlap with data from the literature for single-crystal and polycrystalline samples, while values of *K* fall below previous adiabatic measurements (data taken from: Bell and Rupprecht 1963; Liebermann et al. 1977; Ishidate et al. 1988; Ledbetter et al. 1990; Fischer et al. 1993; Sinelnikov et al. 1998a; Lheureux et al. 1999; Kung and Rigden 1999; Webb et al. 1999). An isothermal value of *K* from compressibility measurements on $CaTiO_3$ (Ross and Angel 1999) is also shown in Figure 2. There is a clear pattern in the variation of shear modulus with increasing $CaTiO_3$ content. Cubic samples (CST100, CST95) have the same values of *G*, within experimental uncertainty. There is then a significant softening over the composition range of tetragonal samples (CST90–CST65). For orthorhombic samples, the shear modulus stiffens markedly over the range CST60–CST50, and then less steeply toward the value for $CaTiO_3$. Variations of the bulk modulus are smaller and subject to a higher degree of scatter. Values for intermediate compositions lie close to a linear extrapolation between the end members, except for CST50 and CST55, which appear to be slightly softer.

**Table 1.** Bulk (*K*) and shear (*G*) moduli of hot-pressed CST pellets, as measured at ambient conditions

| Sample | *K* (GPa) | *G* (GPa) |
|---|---|---|
| CST0 | 167.1 | 105.5 |
| CST10 | 167.3 | 104.2 |
| CST20 | 164.6 | 102.9 |
| CST30 | 165.3 | 101.7 |
| CST40 | 167.7 | 100.3 |
| CST50 | 157.6 | 101.9 |
| CST55 | 158.2 | 98.7 |
| CST60 | 168.0 | 89.7 |
| CST65 | 166.0 | 81.4 |
| CST70 | 164.6 | 81.6 |
| CST75 | 165.9 | 83.1 |
| CST80 | 168.4 | 84.8 |
| CST85 | 169.3 | 88.8 |
| CST90 | 171.9 | 95.1 |
| CST95 | 170.6 | 112.6 |
| CST100 | 168.6 | 112.8 |

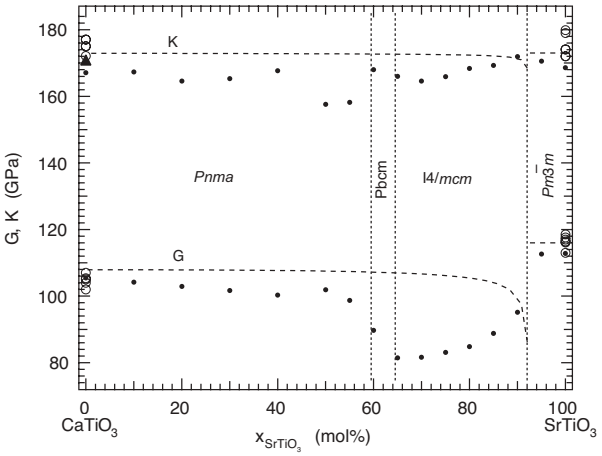


**Figure 2.** Experimental data for bulk and shear moduli (filled circles) obtained in the present study. Vertical dotted lines show the presumed limits of different structure types at room temperature; approximate composition limits for the *Pbcm* structure were taken from Mishra et al. (2006a). Data for $CaTiO_3$ and $SrTiO_3$ from the literature (Bell and Rupprecht 1963; Liebermann et al. 1977; Ishidate et al. 1988; Ledbetter et al. 1990; Fischer et al. 1993; Sinelnikov et al. 1998a; Kung and Rigden 1999; Lheureux et al. 1999; Webb et al. 1999) are shown by open symbols. An isothermal value of *K* from compressibility measurements on $CaTiO_3$ (Ross and Angel 1999) is shown as a filled triangle. Broken lines are variations of calculated elastic properties for cubic and tetragonal CST based on a tricritical model of the cubic ↔ tetragonal transition, taken from Carpenter (2007b).

Experimental data for travel times as a function of oil pressure, acoustic velocities as a function of calibrated pressure and the final bulk moduli as a function of pressure for CST95 and CST65 are listed in Table 2 and displayed in Figure 3. For CST95 there is a clear anomaly at ~100 bars oil pressure in the raw travel time data. This becomes a break in slope in $G$ at ~2 GPa, followed by substantial softening in the range 2–3 GPa. The bulk modulus of CST95 shows a more or less monotonic stiffening with increasing pressure. A $Pm\bar{3}m \leftrightarrow I4/mcm$ transition is expected to occur close to 2 GPa (Carpenter 2007b), and the observed trends in $K$ and $G$ are similar in form to the trends through the transition composition at room temperature (Fig. 2). There is no equivalent anomaly in the raw travel time data for CST65. Instead, distinct changes in the trends of $V_p$ and $V_s$ have been found at ~130 bars oil pressure. These become changes in curvature of $G$ and $K$ at ~2.5–3 GPa.

## Comparison of observed and predicted behavior

### $Pm\bar{3}m \leftrightarrow I4/mcm$ transition as a function of composition

Reasonable agreement between calculated variations and experimental data for the strain behavior of CST0 – CST90 was obtained by Carpenter (2007b) for a tricritical model of the $Pm\bar{3}m \leftrightarrow I4/mcm$ transition. In this limiting case, only the transition temperature, $T_{c2}$, was allowed to vary with composition. The reference elastic constants for cubic samples, strain coupling coefficients, and the principal Landau coefficients were all assumed to be the same as for $SrTiO_3$, except for $\lambda_4$ which was adjusted so as to give $(b_2^* + b_2'^*) = 0$. Calculated excess heat capacities were at least consistent with limited experimental data for CST0 and CST49. Predicted variations of bulk and shear moduli from this model have been added to Figure 2 for comparison with the new experimental data. Values of predicted and observed values of the isotropic Young's modulus, $E$, have

**Table 2.** Ultrasonic data for CST95 and CST65 collected for P- and S-waves in-situ at high pressures

| $P$ (GPa) | Velocity (km·s$^{-1}$) | | $K$ (GPa) | $G$ (GPa) | $P$ (GPa) | Velocity (km·s$^{-1}$) | | $K$ (GPa) | $G$ (GPa) |
|---|---|---|---|---|---|---|---|---|---|
| | P-wave | S-wave | | | | P-wave | S-wave | | |
| CST95 | | | | | CST65 | | | | |
| 0.50 | 7.915 | 4.717 | 166.3 | 112.1 | 0.44 | 7.740 | 4.156 | 174.5 | 81.7 |
| 0.74 | 7.950 | 4.728 | 168.6 | 112.8 | 0.67 | 7.795 | 4.165 | 178.2 | 82.1 |
| 1.04 | 8.006 | 4.736 | 172.6 | 113.3 | 0.90 | 7.807 | 4.179 | 178.6 | 82.8 |
| 1.49 | 8.041 | 4.735 | 176.0 | 113.6 | 1.12 | 7.844 | 4.198 | 180.6 | 83.6 |
| 1.73 | 8.053 | 4.744 | 176.7 | 114.2 | 1.35 | 7.872 | 4.197 | 182.9 | 83.7 |
| 1.97 | 8.067 | 4.734 | 178.8 | 113.9 | 1.57 | 7.903 | 4.213 | 184.7 | 84.4 |
| 2.20 | 8.057 | 4.716 | 179.4 | 113.1 | 1.79 | 7.922 | 4.230 | 185.3 | 85.3 |
| 2.44 | 8.054 | 4.686 | 181.2 | 111.8 | 2.01 | 7.940 | 4.247 | 186.1 | 86.0 |
| 2.68 | 8.047 | 4.648 | 183.3 | 110.2 | 2.22 | 7.959 | 4.256 | 187.2 | 87.0 |
| 2.91 | 8.032 | 4.613 | 184.4 | 108.7 | 2.45 | 7.979 | 4.271 | 188.2 | 87.2 |
| 3.15 | 8.036 | 4.589 | 186.4 | 107.7 | 2.67 | 7.987 | 4.274 | 188.8 | 87.4 |
| 3.38 | 8.044 | 4.565 | 188.9 | 106.7 | 2.88 | 8.008 | 4.279 | 190.2 | 87.7 |
| 3.61 | 8.045 | 4.553 | 189.9 | 106.2 | 3.12 | 8.040 | 4.290 | 192.3 | 88.3 |
| 3.83 | 8.051 | 4.542 | 191.4 | 105.8 | 3.33 | 8.070 | 4.296 | 194.4 | 88.7 |
| 4.05 | 8.052 | 4.532 | 192.2 | 105.6 | 3.54 | 8.090 | 4.292 | 196.4 | 88.6 |
| 4.28 | 8.071 | 4.529 | 194.4 | 105.5 | 3.76 | 8.118 | 4.304 | 198.1 | 89.2 |
| 4.50 | 8.087 | 4.524 | 196.2 | 105.3 | 3.97 | 8.138 | 4.302 | 200.4 | 89.2 |
| 4.72 | 8.093 | 4.519 | 197.2 | 105.2 | 4.19 | 8.158 | 4.299 | 202.2 | 89.1 |
| 4.95 | 8.096 | 4.511 | 198.0 | 105.0 | 4.41 | 8.180 | 4.308 | 203.6 | 89.7 |
| 5.17 | 8.119 | 4.513 | 200.2 | 105.2 | 4.64 | 8.196 | 4.307 | 205.4 | 89.7 |
| 5.39 | 8.121 | 4.511 | 200.3 | 105.2 | 4.85 | 8.209 | 4.313 | 206.1 | 90.0 |
| 5.60 | 8.146 | 4.510 | 203.0 | 105.3 | 5.07 | 8.220 | 4.312 | 207.3 | 90.1 |
| 5.81 | 8.161 | 4.512 | 204.3 | 105.5 | 5.29 | 8.239 | 4.309 | 209.1 | 90.1 |
| 6.02 | 8.165 | 4.498 | 205.7 | 104.9 | 5.50 | 8.275 | 4.309 | 212.1 | 90.1 |
| 6.23 | 8.188 | 4.494 | 208.0 | 104.9 | 5.72 | 8.279 | 4.313 | 212.6 | 90.4 |
| 6.44 | 8.198 | 4.507 | 208.3 | 105.6 | 5.94 | 8.289 | 4.320 | 213.1 | 90.8 |
| 6.66 | 8.192 | 4.500 | 208.3 | 105.3 | 6.16 | 8.309 | 4.321 | 215.1 | 91.0 |
| 6.86 | 8.212 | 4.502 | 210.2 | 105.5 | 6.38 | 8.319 | 4.320 | 215.6 | 91.0 |
| 7.07 | 8.221 | 4.494 | 211.7 | 105.3 | 6.60 | 8.333 | 4.321 | 217.2 | 91.1 |
| 7.27 | 8.237 | 4.502 | 212.9 | 105.7 | 6.82 | 8.340 | 4.328 | 217.8 | 91.5 |
| 7.46 | 8.241 | 4.497 | 213.6 | 105.6 | 7.04 | 8.346 | 4.327 | 218.6 | 91.5 |
| 7.67 | 8.253 | 4.493 | 215.1 | 105.5 | 7.26 | 8.365 | 4.333 | 219.9 | 91.9 |
| 7.86 | 8.269 | 4.498 | 216.4 | 105.8 | 7.47 | 8.375 | 4.329 | 221.2 | 91.9 |
| 8.06 | 8.271 | 4.493 | 217.0 | 105.7 | 7.70 | 8.397 | 4.345 | 222.2 | 92.6 |
| 8.26 | 8.288 | 4.486 | 219.2 | 105.5 | 7.90 | 8.393 | 4.342 | 222.3 | 92.5 |
| 8.46 | 8.297 | 4.487 | 219.9 | 105.7 | 8.12 | 8.399 | 4.345 | 222.7 | 92.7 |
| 8.65 | 8.312 | 4.498 | 220.9 | 106.2 | 8.34 | 8.408 | 4.344 | 223.8 | 92.8 |
| 8.85 | 8.321 | 4.485 | 222.6 | 105.7 | 8.56 | 8.425 | 4.343 | 225.4 | 92.9 |
| 9.04 | 8.327 | 4.490 | 223.2 | 106.1 | 8.78 | 8.422 | 4.347 | 225.2 | 93.1 |
| 9.23 | 8.341 | 4.495 | 223.9 | 106.4 | 9.01 | 8.432 | 4.354 | 225.8 | 93.5 |
| 9.43 | 8.343 | 4.496 | 224.4 | 106.5 | 9.21 | 8.450 | 4.355 | 227.3 | 93.6 |
| 9.62 | 8.351 | 4.497 | 225.3 | 106.6 | 9.43 | 8.445 | 4.355 | 227.3 | 93.7 |
| 9.81 | 8.360 | 4.496 | 226.4 | 106.7 | 9.65 | 8.462 | 4.356 | 228.8 | 93.8 |
| 9.99 | 8.355 | 4.501 | 226.0 | 107.0 | 9.86 | 8.461 | 4.363 | 228.4 | 94.2 |
| 10.18 | 8.370 | 4.496 | 227.7 | 106.9 | 10.07 | 8.475 | 4.370 | 229.5 | 94.6 |
| 10.37 | 8.372 | 4.492 | 228.4 | 106.8 | 10.30 | 8.482 | 4.369 | 230.4 | 94.6 |
| 10.55 | 8.383 | 4.498 | 229.0 | 107.1 | 10.52 | 8.488 | 4.371 | 230.9 | 94.8 |
| | | | | | 10.74 | 8.486 | 4.372 | 231.1 | 95.0 |

*Note:* Data include corrections for bonding between sample and buffer rod and for the effect of changing sample dimensions with pressure.

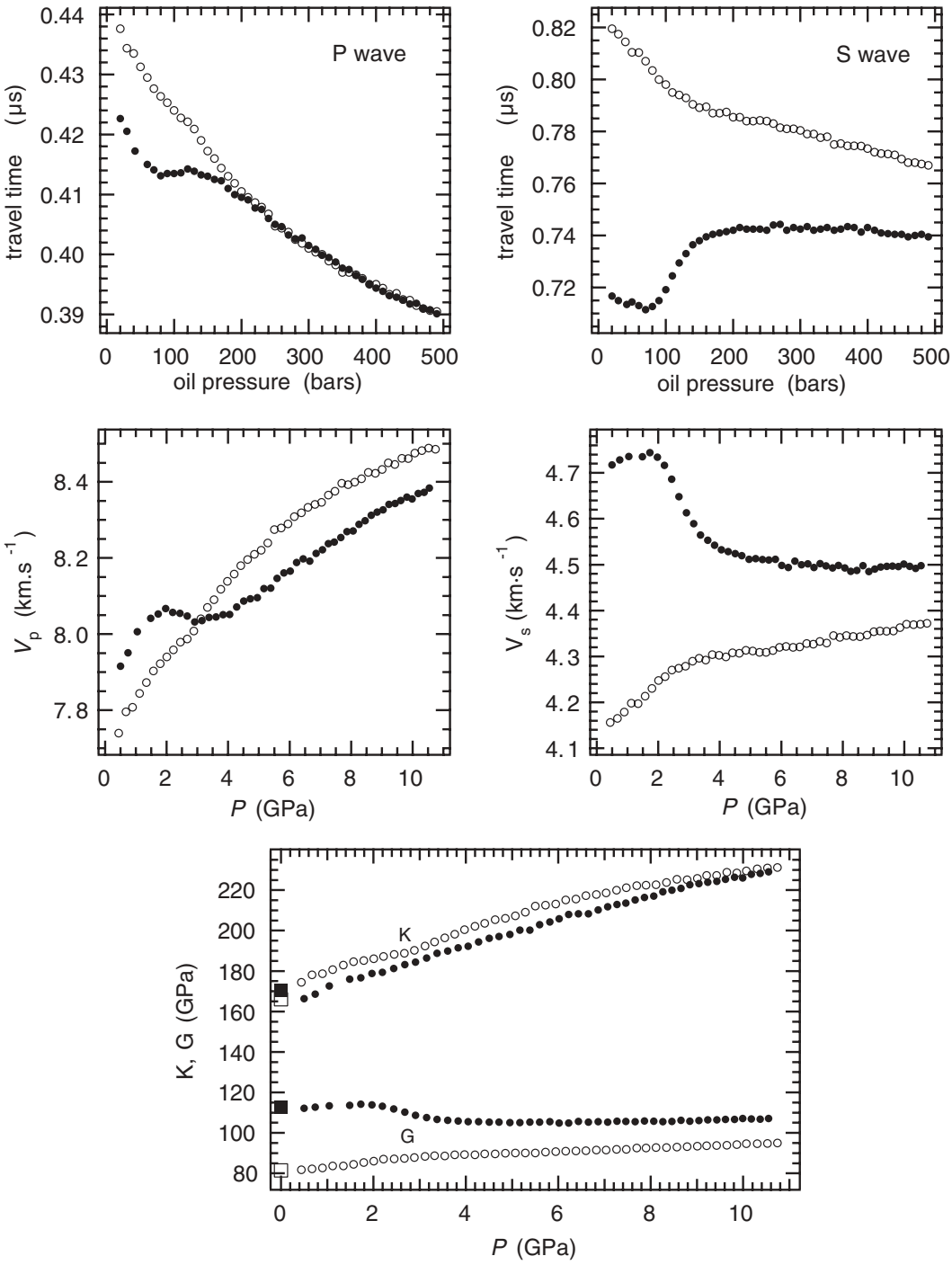


**FIGURE 3.** Ultrasonic data for CST65 (open circles) and CST95 (filled circles) collected in-situ at high pressures. Travel times vs. oil pressure are raw data, with no corrections for changes in sample length at high pressures. Velocity data include pressure calibration, corrections for the effects of gold foil bond between the sample and buffer rod and corrections for the change in sample length, based on the method of Cook (1957).

also been calculated using $E = 9KG/(3K+G)$. In Figure 4, these are compared with the room temperature data of Harrison et al. (2003) for CST55–CST85, as rescaled from relative to absolute values in Carpenter (2007b).

Comparison of experimental and predicted variations of $K$ are consistent with the view that the $Pm\bar{3}m \leftrightarrow I4/mcm$ transition can be responsible only for very limited softening of the bulk modulus. The model predicts softening by ~4.5 GPa at the transition point (CST92) and ~0.1 GPa for compositions (and temperatures) well away from the transition point. Such small variations are due to the weak coupling of volume strain with the order parameter and are below the resolution limit of

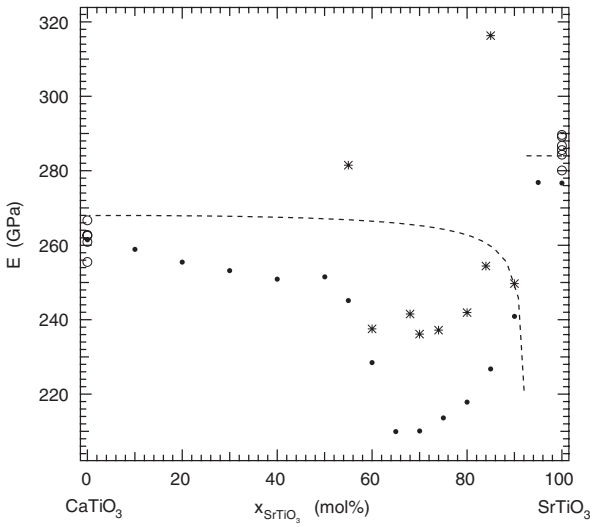


**FIGURE 4.** Variations of Young's modulus (filled circles) as a function of composition at ambient conditions, as calculated from ultrasonic data for $K$ and $G$ given in Figure 2. Open circles are values calculated from literature data for $CaTiO_3$ and $SrTiO_3$ shown in Figure 2. Stars are values of $E$ extracted by Carpenter (2007b) from Dynamical Mechanical Analysis results of Harrison et al. (2003). Broken lines are variations of $E$ calculated from $K$ and $G$ shown in Figure 2 for the tricritical model of the $Pm\bar{3}m \leftrightarrow I4/mcm$ transition.

the experimental data. On the other hand, the shear modulus of tetragonal samples shows a softening of ~20–30 GPa with respect to cubic $SrTiO_3$ and up to ~20 GPa with respect to properties of the tetragonal structure predicted on the basis of the tricritical Landau model. The new experimental data collected at MHz frequencies give a pattern of variation of Young's modulus that parallels the variations extracted from the results of Harrison et al. (2003) for 1 Hz. Both sets of data appear to indicate that experimental softening due to the $Pm\bar{3}m \leftrightarrow I4/mcm$ transition is substantially greater than the softening expected to arise from strain/order parameter coupling alone. Given that this additional softening seems to disappear in orthorhombic CST (Fig. 2), it is logical to suggest that some influence of microstructure in tetragonal samples may be involved. However, the data refer to conditions which are below the freezing interval around ~140 °C, where the transformation twin walls are believed to become pinned by defects (Harrison et al. 2003).

### $Pm\bar{3}m \leftrightarrow I4/mcm$ transition as a function of pressure

To predict the variations of $K$ and $G$ for CST95 at high pressures, it is first necessary to estimate the magnitude of the coupling coefficient, $\lambda_4$, at this composition. The apparent success of a tricritical model for the $Pm\bar{3}m \leftrightarrow I4/mcm$ transition in reproducing strain and heat capacity data for the composition range CST0–CST90 implies that the fourth order coefficient $(b_2^* + b_2'^*)$ could decrease from 0.00081 GPa for $SrTiO_3$ to ~0 for CST92. This change has been ascribed to an increase in the coupling coefficient, $\lambda_4$, from –0.075 to –0.131 GPa, implying stronger coupling between the order parameter and the tetragonal strain. For present purposes it is assumed that $\lambda_4$ varies linearly with composition between CST100 and CST92, giving $\lambda_4$ = –0.11 GPa for CST95. The other coefficients are assumed to remain constant. Since

$$b_2^* + b_2'^* = b_2 + b_2' - \frac{2\lambda_2^2}{\frac{1}{3}\left(C_{11}^o + 2C_{12}^o\right)} - \frac{8\lambda_4^2}{\frac{1}{2}\left(C_{11}^o - C_{12}^o\right)} \quad (1)$$

(from Carpenter 2007a), it follows that $(b_2^* + b'^*_2) = 0.000356$ GPa for CST95.

Gallardo et al. (2003) concluded, on the basis of measurements of excess heat capacity, that the transition is closer to second order [$\Delta S \propto q_4^2 \propto (T_{c2} - T)$] in CST96 than it is in $SrTiO_3$. This is counter to the view being presented here that addition of $CaTiO_3$ to $SrTiO_3$ in solid solution causes the transition to take on progressively more tricritical character. The subsidiary neutron diffraction data of Gallardo et al. have therefore been re-examined. Values of the square of the structure factors for 211 and 213 (superlattice) reflections, $F_{211}^2$ and $F_{213}^2$, were taken from their Figure 2, averaged and replotted. Using their value of $T_{c2}$ = 220 K from the heat capacity measurements, which compares with $T_{c2}$ ~ 214 K for CST96 from Lemanov (1997), the evolution of $q_4^2$ has been calculated using Equation 15 of Carpenter (2007a), with $(b_2^* + b'^*_2) = 0.000356$ and other parameters as for $SrTiO_3$. Figure 5 shows that the data are consistent with $F^2 \propto q_4^2$ (solid line) calculated in this way. Also shown in Figure 5 is the evolution of $q_4^2$ for a solution which has all the parameters of $SrTiO_3$ except for $T_{c2}$ = 220 K (broken line), though this largely remains within the experimental error bars. Gallardo et al. suggested that their sample might have contained some chemical heterogeneity, with the result that a 246 or tricritical heat capacity anomaly through the transition would have been smeared out. A definitive determination of order parameter evolution requires higher resolution data, but Figure 5 is at least permissive of the view that values of $(b_2^* + b'^*_2)$ reduce with increasing $CaTiO_3$ content at Sr-rich compositions in the CST solid solution.

Linear interpolation between experimental values of Bianchi (1996) in Lemanov (1997) for the cubic ↔ tetragonal transition temperature at CST94 and CST96 gives $T_{c2}$ = 234 K for CST95. The transition pressure as a function of $T_{c2}$, given by

$$P_c = \frac{a_2 \Theta_{s2} \frac{1}{3}\left(C_{11}^o + 2C_{12}^o\right)}{2\lambda_2}\left(\coth\left(\frac{\Theta_{s2}}{T}\right) - \coth\left(\frac{\Theta_{s2}}{T_{c2}}\right)\right), \quad (2)$$

then yields $P_c$ = 2.11 GPa for CST95 at 295 K (using values of all the other parameters from Table 6 of Carpenter 2007a). The solution for $q_4$ as a function of pressure (Carpenter 2007b) at 295 K is

$$q_4^2 = \frac{-\left(b_2^* + b_2''^*\right) + \sqrt{\left(b_2^* + b_2''^*\right)^2 + 4\frac{2\lambda_2}{\frac{1}{3}\left(C_{11}^o + 2C_{12}^o\right)}\left(c_2 + c_2''\right)\left(P - P_c\right)}}{2\left(c_2 + c_2''\right)}. \quad (3)$$

Inverse susceptibilities, $\chi_4^{-1}$ and $\chi_6^{-1}$, and the elastic constants are given by the expressions listed in Table 2 of Carpenter (2007a). Hill averages of the Voigt/Reuss limits (Hill 1952) for the softening of the bulk and shear moduli are therefore readily obtained. This softening is relative to the bulk and shear moduli of cubic CST95 ($K^o$ and $G^o$) extrapolated to high pressures, which have been determined by applying linear fits to the experimental data: $K^o = 166.11 + 6.372\,P$ GPa (fit to data in the range 1.0–2.0

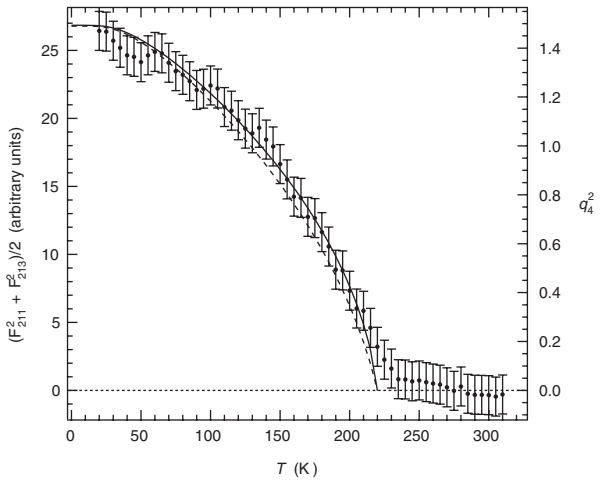


**FIGURE 5.** Average values of squares of the structure factors of 211 and 213 reflections, $F^2_{211}$ and $F^2_{213}$ (left axis), from neutron diffraction data of Gallardo et al. (2003) for CST96 scale with $q_4^2$ (right axis) as calculated using Equation 15 of Carpenter (2007a). The solid line was calculated with $T_{c2}$ = 220 K, $(b_2^* + b'^*_2)$ = 0.000356 GPa and other parameters as listed in Table 6 of Carpenter (2007a) for $SrTiO_3$. The broken line is the calculated variation of $q_4^2$ with $T_{c2}$ = 220 K and all other parameters as for $SrTiO_3$, with an additional scaling factor of 1.13 applied to the calculated values of $q_4^2$ to produce overlap with data points for $\frac{1}{2}\left(F^2_{211} + F^2_{213}\right)$.

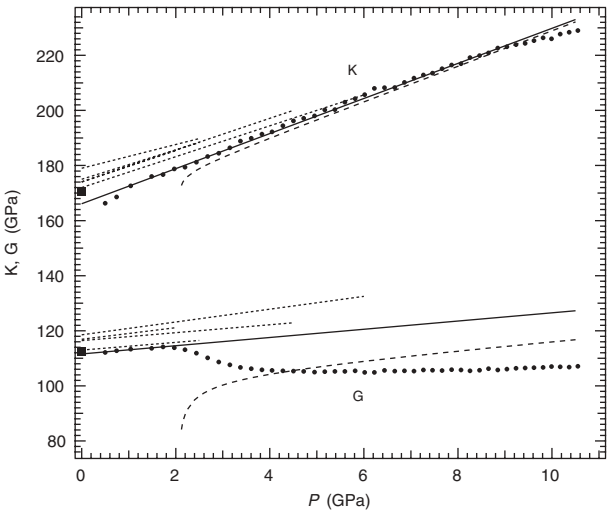


**FIGURE 6.** Comparison of observed and calculated variations of bulk and shear moduli as a function of pressure for CST95. Filled circles are data from Figure 3. Filled squares are room-pressure values from Figure 2. Solid lines are fits to the data over pressure intervals 1.0–2.0 GPa for $K$ and 0.5–1.7 GPa for $G$, representing the bulk elastic properties of cubic CST95. For comparison, the trends of bulk and shear moduli from the literature for $SrTiO_3$ (Beattie and Samara 1971; Ishidate et al. 1988; Fischer et al. 1989, 1993; Lheureux et al. 1999) are shown as dotted lines. Broken lines are the calculated variations of $K$ and $G$ for CST95 with $\lambda_4$ = –0.11 GPa and $P_c$ = 2.11 GPa.

GPa), $G^o$ = 111.55 + 1.495 $P$ GPa (fit to data in the range 0.5–1.7 GPa), as shown in Figure 6.

Fits to the low-pressure data and calculated softening in the stability field of the tetragonal phase are compared with the experimental data for CST95 in Figure 6. Calculated and observed variations of the bulk modulus are consistent in showing little or no influence of the cubic ↔ tetragonal transition. Calculated and observed variations of the shear modulus are in agreement to the extent that the substantial softening associated with the cubic ↔ tetragonal transition starts to develop close to the predicted transition pressure of 2.11 GPa. The data do not show the characteristic discontinuity at $P = P_c$ for second order and tricritical transitions, however. Rather, the observed softening increases smoothly away from the transition point and then becomes greater than is predicted for the effects of strain/order parameter coupling alone. This is similar to the behavior as a function of composition through the transition. The influence of twin wall motions is again suspected, even though temperature was below the domain wall freezing interval of Harrison et al. (2003).

### Anelastic behavior of tetragonal CST

Experimental data for the shear modulus as a function of composition at ambient conditions and as a function of pressure in CST95 suggest that there may be some additional softening beyond what is expected from strain/order parameter coupling in tetragonal samples. The total softening, expressed as the difference between the observed values for the tetragonal phase and extrapolated values for the cubic phase, $\Delta G$, scales approximately linearly with the calculated values of $q_4$ for both composition and pressure as the external variables (Figs. 7a and 7b). This relationship implies that the softening depends in some regular manner on distance from the transition point, though it has not been considered before. Anelastic contributions of the twin walls may well be implicated.

Separate contributions of twin wall motions and strain/order parameter couplings are not additive for the elastic constants but they are additive for compliances. Following Schranz et al. (1999), Kityk et al. (2000a, 2000b), and Carpenter (2007b), the compliance, $S$, of tetragonal CST is given by

$$S = S^o + \Delta S_L + \Delta S_W \quad (4)$$

where $S^o$ is the compliance of the cubic reference structure, $\Delta S_L$ is the change in compliance due to strain/order parameter coupling, and $\Delta S_w$ is the change in compliance due to the effect of twin wall motions. Schranz et al. (1999) and Kityk et al. (2000a, 2000b) suggested that $\Delta S_w$ varies linearly with $q_4^2$ in single crystals through a dependence on the tetragonal shear strain. The new calibration of Landau parameters also gives results consistent with this simple model for the case of elasticity measurements made at low frequencies (Carpenter 2007b). Experimental data for the shear modulus of polycrystalline samples obtained at high frequencies in the present study have therefore been considered as $S = 1/G$, with the implicit assumption that the phase angle between applied stresses and resultant strains is relatively small. These have then been compared with fits of the form $S = (S^o + \Delta S_L) + Aq_4^2$. Here $(S^o + \Delta S_L)$ has been taken as $1/(G^o + \Delta G_L)$, where $\Delta G_L$ is the softening calculated for strain/order parameter coupling. Some agreement is obtained away from the transition point for $A$ = 0.00106 GPa$^{-1}$ in the case of variable composition (Fig. 7c), but the comparison is much less convincing for the

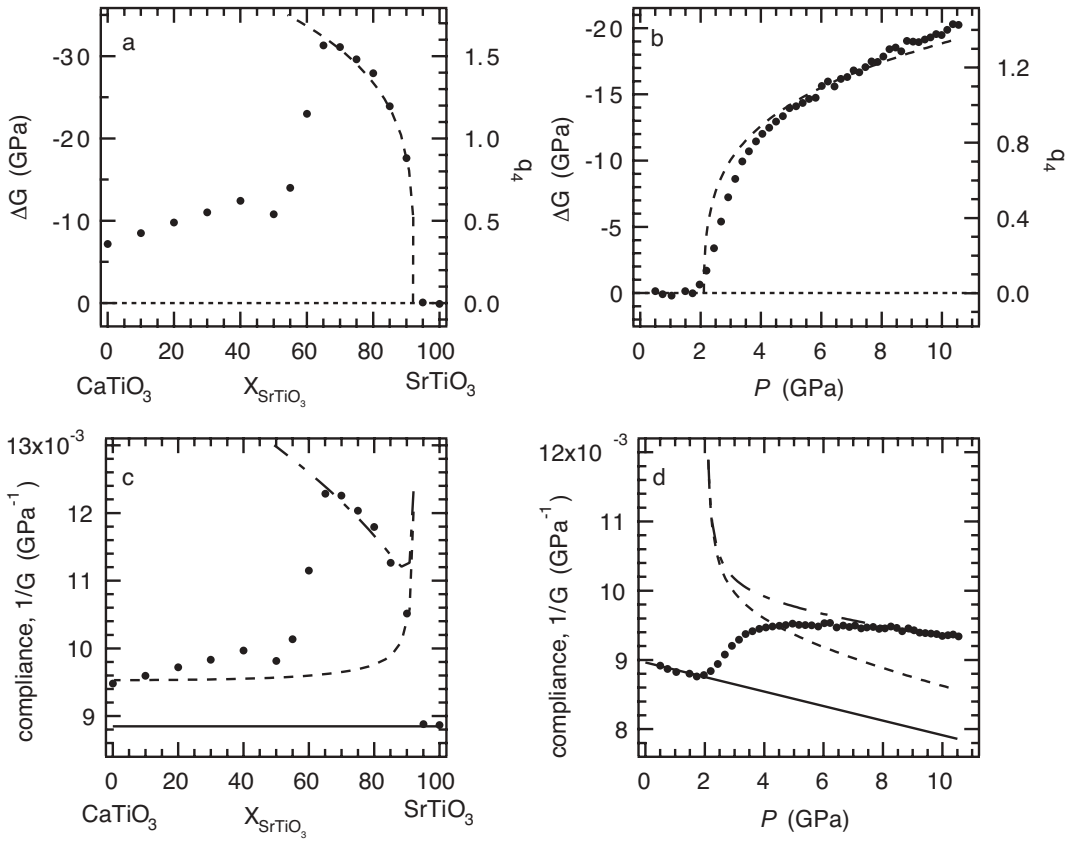


**FIGURE 7.** Possible anelastic contributions to the softening of tetragonal CST. (**a**) The change in shear modulus, $\Delta G$, was taken as the difference between observed shear modulus values and a constant value for cubic CST. In the compositional range of tetragonal CST, this scales approximately with $q_4$ for the tricritical Landau model with $\lambda_4 = -0.131$ GPa (broken line, right axis). (**b**) The difference of shear modulus between cubic and tetragonal CST95 as a function of pressure scales approximately with $q_4$ from a Landau model with $\lambda_4 = -0.11$ GPa (broken line, right axis). (**c**) Model for compliance as a function of composition based on Equation 4. The solid line is $1/G^o$ for cubic CST, using $G^o = 113$ GPa. The broken line is $1/(G^o + \Delta G_L)$, representing the compliance for a polycrystalline sample in which the only softening is due to strain/order parameter coupling. The dot dash line is a fit to the data that has $S = 1/(G^o + \Delta G_L) + 0.00106\ q_4^2$. (**d**) The same model as in **c**, but with pressure as the external variable for CST95. The solid line is $1/G^o$ and the broken line is $1/(G^o + \Delta G_L)$. The dot-dash line is a fit with $S = 1/(G^o + \Delta G_L) + 0.0004\ q_4^2$.

case of variable pressure ($A = 0.0004$ GPa$^{-1}$, Fig. 7d).

The extent of softening in polycrystalline samples of CST perovskite at tens of MHz is less than shown by single crystals of $SrTiO_3$ in selected orientations at ~10 Hz (Schranz et al. 1999; Kityk et al. 2000a, 2000b). This must be due, at least in part, to the averaging effect of multiple grain orientations. Only a proportion of individual crystals will have twin walls aligned optimally with respect to the externally applied shear stress so as to undergo maximum possible displacement. Many grains will have twin walls that do not move because they are aligned normal to the external stress, and some may have twin wall orientations that actually result in stiffening (e.g., see Fig. 10c of Carpenter 2007b). The total increase in $S$ will be some integral over all orientations. However, such averaging is unlikely to be responsible for differences between the calculated and observed variations close to the transition point. The lack of any discontinuity in $G$ or $S$ suggests that, in this interval, either the strain/order parameter coupling model is inadequate for describing phase transitions in polycrystalline samples or that the anelastic contribution of the twin walls to the compliance is more profound than a simple dependence on the spontaneous strain and $q_4^2$ allows. Whichever is the case, the relationship $\Delta G \propto q_4$ provides an empirical description of the combined influence of the two contributions.

### *I*4/*mcm* ↔ *Pnma* transition

A quantitative model has not yet been developed for the first order *I*4/*mcm* ↔ *Pnma* transition in CST perovskites. The likely form of elastic softening that might accompany this transition can be examined qualitatively using the expressions in Table 5 of Carpenter (2007a). Strictly speaking, the averages of Voigt and Reuss limits (or Hashin-Strikman bounds) should be used to describe the properties of polycrystalline samples but the Voigt limit gives simple expressions that permit the contributions of separate terms to be visualized most easily. For a $Pm\bar{3}m$ ↔ *Pnma* transition the order parameter components with non-zero values are $q_2$ and $q_4$ (= $q_6$). The Voigt limits for bulk and shear moduli are

$$K_V = \frac{1}{3}\left(C_{11}^o + 2C_{12}^o\right) - 4\lambda_1^2\chi_2 q_2^2 - 8\lambda_2^2\chi_4 q_4^2 \quad (5)$$

$$G_V = \frac{1}{5}\left(C_{11}^o - C_{12}^o + 3C_{44}^o\right) - \frac{2}{5}\left(8\lambda_3^2\chi_2 + 3\lambda_6 + 2\lambda_7\right)q_2^2 - \frac{2}{5}\left(16\lambda_4^2\chi_4 + \lambda_5^2\chi_4 + \lambda_5^2\chi_5\right)q_4^2 \ . \quad (6)$$

In this model, the total softening is the sum of contributions from the separate M and R point transitions, $Pm\bar{3}m \leftrightarrow P4/mbm$ and $Pm\bar{3}m \leftrightarrow Imma$.

For the $Pm\bar{3}m \leftrightarrow Imma$ component of the *Pnma* structure, $q_4$ will be approximately half the value of $q_4$ for the $Pm\bar{3}m \leftrightarrow I4/mcm$ transition (see Eqs. 15 and 16 of Carpenter 2007a). The contribution of terms in $q_4^2$ to $G_V$ and $K_V$ will therefore be approximately the same for the *Imma* structure as they are for the *I*4/*mcm* structure. It is then necessary only to consider the additional contributions of a $Pm\bar{3}m \leftrightarrow P4/mbm$ transition. If the latter is thermodynamically continuous, the transition temperature ($T_{c1}$ in Eq. 1 of Carpenter 2007a) will be between the transition temperatures for the $Pm\bar{3}m \leftrightarrow I4/mcm$ and $I4/mcm \leftrightarrow Pnma$ transitions (see Fig. 2 of Carpenter 2007a). If the transition is also close to tricritical in character, the evolution of $q_2$ will not be dissimilar from the evolution of $q_4$. The volume strain of *Pnma* structures at intermediate compositions in the CST solid solution is small (Carpenter et al. 2001), so the coupling coefficients $\lambda_1$ and $\lambda_2$ must both be small. Any anomaly in the bulk modulus at the $I4/mcm \leftrightarrow Pnma$ transition is, therefore, also expected to be small.

The tetragonal strain for *Pnma* structures is given by

$$e_{tx} = -\frac{2\left(\lambda_3 q_2^2 - \lambda_4 q_4^2\right)}{\frac{1}{2}\left(C_{11}^o - C_{12}^o\right)} \quad (7)$$

where $e_{tx}$ is a tetragonal strain defined as $e_{tx} = \frac{1}{\sqrt{3}}\left(2e_1 - e_2 - e_3\right)$ (Carpenter et al. 2001). At room temperature $e_{tx}$ for the *Pnma* structure of CST is small and negative (Carpenter et al. 2001), which means that $\lambda_3$ and $\lambda_4$ have values that are similar in magnitude. The contributions of coupling of the order parameter with strains $e_4$ and $e_5$ is different for the M and R point octahedral tilting transitions, with the result that the coupling coefficients $\lambda_5$ (for *Imma*) and $\lambda_6$, $\lambda_7$ (for *P*4/*mbm*) appear as different terms in expressions for the elastic softening. $C_{44}$ has a substantial discontinuity at $T_c$ for the $Pm\bar{3}m \leftrightarrow I4/mcm$ transition (see Table 2 and Fig. 3 of Carpenter 2007a), whereas it should decrease (or increase, depending on the signs of $\lambda_6$ and $\lambda_7$) linearly with $q_2^2$ (see Table 4 of Carpenter 2007a). If $q_4$ does not vary substantially at the transition point, the discontinuity in $G_V$ at the $I4/mcm \leftrightarrow Pnma$ transition should thus be that due to $-\frac{2}{5}(8\lambda_3^2 q_2^2)$ alone. This should be less than the step in $G_V$ at the $Pm\bar{3}m \leftrightarrow I4/mcm$ transition, which is due to $-\frac{2}{5}(8\lambda_4^2\chi_4 + \lambda_5^2\chi_6)q_4^2$. The form of shear modulus variations as a function of composition across the solid solution at room temperature is thus expected to be as shown in Figure 1. The *Pnma* structure indeed appears to have values of the shear modulus that are below those calculated for the *I*4/*mcm* structure, but it should be noted that there is considerable uncertainty in how the baseline value, $G^o$, of cubic CST varies across the solid solution. The fact that the *I*4/*mcm* structure at CST65–CST90 is observed to be softer instead of stiffer than the *Pnma* structure at CST0–CST55 could then be understood as being due to the additional influence of twin wall motions in tetragonal crystals. There is no evidence for twin wall induced anelastic softening of orthorhombic CST at high temperatures (Harrison et al. 2003) or at room temperature (this study). CST60, which is presumed to have the *Pbcm* structure, appears to have a smaller shear modulus than CST0–CST55.

Elastic softening associated with a transition from *I*4/*mcm* to *Pnma* symmetry in CST65 would also be expected to have the form shown in Figure 1, but this is quite different from what is actually observed. According to Yamanaka et al. (2002) the $I4/mcm \leftrightarrow Pnma$ transition occurs between room pressure and 3.5 GPa. These authors may not have searched systematically for weak superlattice reflections that distinguish the *Pbcm* structure from the *Pnma* structure, and another possibility is that the elastic anomalies are due to a transition $I4/mcm \leftrightarrow Pbcm$. A formal analysis of such a transition has not yet been attempted. Kinks in the trends of both *K* and *G* between 2 and 3 GPa might also be explained more simply in terms of changes in compression mechanism without a change in symmetry.

At pressures and temperatures that are well away from the transition temperatures, softening due to strain/order parameter coupling in *Pnma* structures becomes effectively constant for the contribution from $Pm\bar{3}m \leftrightarrow Imma$ and, if $\lambda_6$ and $\lambda_7$ are small, only weakly dependent on $q_2^2$ for the contribution from $Pm\bar{3}m \leftrightarrow P4/mbm$.

## Discussion

Landau theory developed for all M and R point transitions in perovskites (Carpenter 2007a) has allowed a parameterization that leads to detailed and quantitative descriptions of the elastic properties of untwinned crystals of $SrTiO_3$. Modification of only a few parameters then allows the development of models for the elastic behavior across the entire CST solid solution (Carpenter 2007b). The approach can be applied equally to second order, tricritical, and first order phase transitions, though there is a general tendency for tilting transitions in perovskites to be close to tricritical in character. The Landau expansions do not as yet explain why the *Pnma* structure is more stable than the *Cmcm* structure, but one possibility is that some of the strain/order parameter coupling coefficients are subtly different for the two structures. Two important limitations of the models are that the composition dependence of the coupling coefficient $\lambda_5$ is not known, and that the composition dependence of elastic properties for cubic CST is known only for the most Sr-rich compositions. Further measurements of elastic properties as a function of temperature are required to refine the values of these parameters and would also allow the composition dependence of other parameters in the Landau expansion to be investigated.

The present approach of using polycrystalline samples to determine absolute values of bulk elastic properties of CST perovskites directly has revealed that, in contrast with the relatively smooth variation of bulk modulus, the shear modulus shows unusual and substantial anomalies as functions of composition and pressure through the stability fields of cubic, tetragonal and orthorhombic structures. Of the two limiting cases considered in Carpenter (2007b), the tricritical model of the $Pm\bar{3}m \leftrightarrow I4/mcm$ transition for CST0–CST90 gives the best representation of observed strain behavior. This model has then led to the hypothesis that the anomalous evolution of *G* can be

understood in terms of strain/order parameter coupling in *Pnma* and *I*4/*mcm* structures combined with anelastic contributions of twin wall motions in samples with *I*4/*mcm* symmetry. In the absence of twin wall effects, the sequence $Pm\bar{3}m \leftrightarrow I4/mcm \leftrightarrow$ *Pnma* would be accompanied by stepwise softening of *G* by up to ~25%. Nonlinear variations in the stability field of the low symmetry phase immediately below each transition point would be due to approximately tricritical character for the M and R point instabilities. The involvement of twin walls could cause *I*4/*mcm* phases to become softer than *Pnma* phases, counter to the normal expectation for classical elastic softening at improper ferroelastic transitions. The same constraints should apply to the elastic behavior as a function of temperature but, as a cautionary note, it should be stressed that assumptions underlying the Landau model for softening in *Pnma* structures remain to be tested.

The new results for elastic softening in polycrystalline tetragonal CST obtained at MHz frequencies provide interesting parallels with the results of Harrison et al. (2003) obtained at 1 Hz. At high temperatures within the *I*4/*mcm* stability field, anelastic softening is believed to involve both rotations of twin walls and the advance or retraction of needle-tipped twins. This gives a large reduction of Young's modulus that is independent of temperature (Harrison and Redfern 2002; Harrison et al. 2003, 2004a, 2004b, 2004c). Below ~140 °C, the softening is substantially diminished in a way that can be understood in terms of pinning of the walls by defects. Harrison and Redfern (2002) also found that anelastic effects can be induced below the pinning temperature interval in $LaAlO_3$ by the application of stresses that exceed the critical stress needed to separate twin walls from their pinning points. Below the domain wall freezing temperature, some anelastic softening still seems to occur in $SrTiO_3$ and CST at both high and low frequencies (Schranz et al. 1999; Kityk et al. 2000a, 2000b; Binder and Knorr 2001; Lemanov et al. 2002; Carpenter 2007b; this study). Lemanov et al. (2002) concluded that, in response to externally applied elastic stresses, twin walls in $SrTiO_3$ relax on a time scale that can vary between $10^{-2}$ and $10^{-10}$ seconds. In the present study, the pattern of elastic softening shown by polycrystalline CST samples at room temperature seems to be more or less the same at MHz frequencies as it is at ~1 Hz (Fig. 4). If the calibration of Young's modulus applied in Carpenter (2007b) to the data of Harrison et al. (2003) is approximately correct, it follows that dispersion across this range of frequencies may indeed be limited. There is also no evidence in any of the room temperature data that some critical stress must be exceeded before the walls can move. If the walls are truly pinned at fixed points by defects, some other mechanism, such as localized bowing between pinning points, might operate. Whatever the mechanism is, it must also be capable of responding to stress with short relaxation times.

Overall softening of polycrystalline CST samples does not conform to the same simple dependence on spontaneous strain as seems to apply for single crystals of $SrTiO_3$ (Schranz et al. 1999; Kityk et al. 2000a, 2000b; Carpenter 2007b). In particular, the sharp discontinuity at the transition point is lost (Figs. 7c and 7d). Some smearing of elastic properties through the transition point is inevitable for a polycrystalline sample because impinging grain boundaries must prevent a proportion of the strain relaxation associated with the phase transition from occurring. Effective strain/coupling coefficients will then be smaller than the equilibrium values and the difference will be most marked when the change in spontaneous strain is greatest, i.e., just below the transition point of a tricritical transition. Some of this smearing would disappear in samples annealed at temperatures just below $T_c$ for long enough to allow grain boundaries to re-adjust to equilibrium strain relaxations of the individual crystals. The empirical relationship shown by the data for both composition and pressure as the external variable, $\Delta G \propto q_4$ (Figs. 7a and 7b), seems to be too well defined for smearing by inhomogeneous strain effects alone to be the sole cause of the difference between observed and calculated variations, however. Further analysis is clearly required to understand the integration of twin-related softening over all orientations of individual single crystals in a polycrystalline sample with respect to a single orientation of applied stress. Furthermore, the width of twin walls and, hence, their volume fraction, is known to increase substantially as a critical point is approached (Hayward et al. 1996; Chrosch and Salje 1999; Salje et al. 2004), with the possibility that real elastic behavior becomes dominated by the properties of the walls rather than the properties of the material between the walls.

The new high-frequency data are consistent with the view, proposed by Harrison et al. (2003) on the basis of low-frequency measurements, that twin walls do not influence the elastic behavior of polycrystalline samples of CST with the *Pnma* structure. This difference from the behavior of tetragonal samples could be due to static or dynamic effects (or both). A possible static explanation relates to how M and R point tilts contribute to tetragonal strains. Octahedral tilting at the R point instability produces a positive strain while tilting at the M point instability induces a tetragonal strain in exactly the opposite direction (Eq. 7). The outcome for CST samples is that the total tetragonal strain is close to zero (Carpenter et al. 2001). The strain contrast between adjacent domains is therefore small and the strain induced by moving a twin wall in response to a given stress is also smaller than would occur in a tetragonal sample, as discussed also by Harrison et al. (2003). A dynamical origin for the different behavior might relate to the existence of coupling between the separate order parameters of the *Pnma* structure. Twin wall mobility requires a rapid relaxation of the octahedral tilts in response to applied stress. For $q_4$ alone (*I*4/*mcm*), the relaxation time is certainly small. Once the second order parameter becomes involved, the relaxation process requires two separate tilts, via coupling terms of the form $\lambda q_2^2 q_4^2$ and $\lambda q_2^2 q_4^4$ (Carpenter 2007a). The time scale for such a coupled tilting process need not be as rapid as for the individual tilts operating alone. This issue is also relevant in the context of whether the softening in *Pnma* structures arises by addition of separate coupling of each of the $q_2$ and $q_4$ to the strains or by coupling of the strains to a single effective order parameter that includes both $q_2$ and $q_4$ in fixed proportions.

Even though the observed patterns of elastic softening in CST perovskites are quite unexpected, the models developed to describe them lead to some predictions of the possible elastic behavior of $(Mg,Fe)SiO_3$ and $CaSiO_3$ perovskites. Firstly, the observed phenomenology should be generally the same for all tilting transitions in perovskites, and there is no obvious reason to expect that the silicate phases should be fundamentally dif-

ferent. Thus, the bulk modulus is expected to evolve more or less smoothly with temperature, pressure, and composition, with only small discontinuities at the cubic ↔ tetragonal and tetragonal ↔ orthorhombic transitions. There remains the possibility that the coupling coefficients relating volume strains to the order parameter components themselves vary with $P$, $T$, or composition. This coupling is weak, however, and irregularities in the contribution of strain/order parameter coupling to the bulk modulus will probably remain small. Twin wall motions should not contribute to attenuation effects associated with the bulk modulus. (Mg,Fe)$SiO_3$ with the *Pnma* structure will have a lower value of shear modulus than the equivalent cubic structure at the same pressure and temperature. For pressures and temperatures that are well away from the tetragonal ↔ orthorhombic transition point, the amount of softening is more or less independent of $q_4$. Attenuation effects will only be those arising from standard effects, such as movements at grain boundaries. On the other hand, it must be anticipated that the shear modulus of twinned tetragonal $CaSiO_3$ will be softer than for either cubic or orthorhombic $CaSiO_3$. The form of this variation might be expected to follow the dot-dash line in Figure 1 rather than the solid line for the $I4/mcm$ structure. At seismic frequencies the shear modulus will be strongly affected by the $Pm\bar{3}m \leftrightarrow I4/mcm$ transition, even if $P$, $T$ conditions within the mantle are substantially away from the equilibrium transition point. The contribution of softening due to strain/order parameter coupling will converge to a more or less fixed value away from the transition point but the contribution of anelastic effects could give $G$ an additional pressure and temperature dependence, which will be accompanied by significant attenuation effects. If mantle conditions are below the domain wall freezing regime, the additional softening could scale with $q_4$ and the octahedral tilt angle. If conditions are above the wall freezing regime, the much larger temperature independent softening behavior described by Harrison and Redfern (2002) and Harrison et al. (2003) might occur.

## ACKNOWLEDGMENTS

All the experimental work presented in this paper was completed by P. Sondergeld, with funding from the Natural Environment Research Council (grant number NER/A/S/2000/01055, to MAC). Hot pressing and ultrasonic experiments were undertaken in the Stony Brook High Pressure Laboratory, with partial support of NSF grants to BL (EAR0003340) and to RCL (EAR02-29704).

## REFERENCES CITED

Ball, C.J., Begg, B.D., Cookson, D.J., Thorogood, G.J., and Vance, E.R. (1998) Structures in the system $CaTiO_3/SrTiO_3$. Journal of Solid State Chemistry, 139, 238–247.

Beattie, A.G. and Samara, G.A. (1971) Pressure dependence of the elastic constants of $SrTiO_3$. Journal of Applied Physics, 42, 2376–2381.

Bell, R.O. and Rupprecht, G. (1963) Elastic constants of strontium titanate. Physical Review, 129, 90–94.

Bianchi, U. (1996) Glasartiges Verhalten, Ferroelektrizität und photoinduzierte Effekte in Strontium-Kalzium-Titanit ($Sr_{1-x}Ca_xTiO_3$, $0 \le x \le 0.12$). Ph.D. thesis, Gerhard-Marcator University, Duisburg.

Binder, A. and Knorr, K. (2001) Shear elasticity and ferroelastic hystersis of the low-temperature phase of $SrTiO_3$. Physical Review B, 63, 094106.

Carpenter, M.A. (2007a) Elastic anomalies accompanying phase transitions in (Ca,Sr)$TiO_3$ perovskites: Part I. Landau theory and a calibration for $SrTiO_3$. American Mineralogist, 92, 309–327.

——— (2007b) Elastic anomalies accompanying phase transitions in (Ca,Sr)$TiO_3$ perovskites: Part II. Calibration for the effects of composition and pressure. American Mineralogist, 92, 328–343.

Carpenter, M.A., Becerro, A.I., and Seifert, F. (2001) Strain analysis of phase transitions in (Ca,Sr)$TiO_3$ perovskites. American Mineralogist, 86, 348–363.

Chrosch, J. and Salje, E.K.H. (1999) Temperature dependence of the domain wall width in $LaAlO_3$. Journal of Applied Physics, 85, 722–727.

Cook, R.K. (1957) Variation of elastic constants and static strains with hydrostatic pressure: a method for calculation from ultrasonic measurements. Journal of the Acoustical Society of America, 29, 445–449.

Darling, K.L., Gwanmesia, G.D., Kung, J.F., Li, B., and Liebermann, R.C. (2004) Ultrasonic measurements of the sound velocities in polycrystalline San Carlos olivine in multi-anvil, high-pressure apparatus. Physics of the Earth Planetary Interiors, 143–144, 19–31.

Decremps, F., Zhang, J., Li, B., and Liebermann, R.C. (2001) Pressure-induced softening of shear modes in ZnO. Physical Review B, 63, 224105.

Edwards, L.R. and Lynch, R.W. (1970) The high pressure compressibility and Grüneisen parameter of strontium titanate. Journal of Physics and Chemistry of Solids, 31, 573–574.

Fischer, G.J., Wang, Z., and Karato, S.-I. (1993) Elasticity of $CaTiO_3$, $SrTiO_3$ and $BaTiO_3$ perovskites up to 3.0 GPa: the effect of crystallographic structure. Physics and Chemistry of Minerals, 20, 97–103.

Fischer, M., Bonnello, B., Polian, A., and Léger, J.-M. (1989) Elasticity of $SrTiO_3$ perovskite under high pressure. In A. Navrotsky and D.J. Weidner, Eds., Perovsite: a structure of great interest to Geophysics and Materials Science. Geophysical Monograph, 45, 125–130.

Gallardo, M.C., Becerro, A.I., Romero, F.J., del Cerro, J., Seifert, F., and Redfern, S.A.T. (2003) Cubic-tetragonal phase transition in $Ca_{0.04}Sr_{0.96}TiO_3$: a combined specific heat and neutron diffraction study. Journal of Physics: Condensed Matter, 15, 91–100.

Gwanmesia, G.D. and Liebermann, R.C. (1992) Polycrystals of high-pressure phases of mantle minerals: hot pressing and characterization of physical properties. In Y. Syono and M.H. Manghnani, Eds., High Pressure Research: Application to Earth and Planetary Sciences, 67, p. 117–135. Geophysical Monograph Series, AGU, Washington, D.C.

Gwanmesia, G.D., Li, B., and Liebermann, R.C. (1993) Hot pressing of polycrystals of high-pressure phases of mantle minerals in multi-anvil apparatus. Pure and Applied Geophysics, 141, 467–484.

Harrison, R.J. and Redfern, S.A.T. (2002) The influence of transformation twins on the seismic-frequency elastic and anelastic properties of perovskite: dynamical mechanical analysis of single crystal $LaAlO_3$. Physics of the Earth and Planetary Interiors, 134, 253–272.

Harrison, R.J., Redfern, S.A.T., and Street, J. (2003) The effect of transformation twins on the seismic-frequency mechanical properties of polycrystalline $Ca_{1-x}Sr_xTiO_3$ perovskite. American Mineralogist, 88, 574–582.

Harrison, R.J., Redfern, S.A.T., and Salje, E.K.H. (2004a) Dynamical excitation and anelastic relaxation of ferroelastic domain walls in $LaAlO_3$. Physical Review B, 69, 144101.

Harrison, R.J., Redfern, S.A.T., and Bismayer, U. (2004b) Seismic-frequency attenuation at first-order phase transitions: dynamical mechanical analysis of pure and Ca-doped lead orthophosphate. Mineralogical Magazine, 68, 839–852.

Harrison, R.J., Redfern, S.A.T., Buckley, A., and Salje, E.K.H. (2004c) Application of real-time, stroboscopic X-ray diffraction with dynamical mechanical analysis to characterize the motion of ferroelastic domain walls. Journal of Applied Physics, 95, 1706–1717.

Hayward, S.A., Chrosch, J., Salje, E.K.H., and Carpenter, M.A. (1996) Thickness of pericline twin walls in anorthoclase: an X-ray diffraction study. European Journal of Mineralogy, 8, 1301–1310.

Hill, R. (1952) The elastic behaviour of a crystalline aggregate. Proceedings of the Physical Society of London A, 65, 349–354.

Howard, C.J., Withers, R.L., and Kennedy, B.J. (2001) Space group and structure for the perovskite $Ca_{0.5}Sr_{0.5}TiO_3$. Journal of Solid State Chemistry, 160, 8–12.

Howard, C.J., Withers, R.L., Zhang, Z., Osaka, K., Kato, K., and Takata, M. (2005) Space-group symmetry for the perovskite $Ca_{0.3}Sr_{0.7}TiO_3$. Journal of Physics: Condensed Matter, 17, L459–465.

Ishidate, T., Sasaki, S., and Inoue, K. (1988) Brillouin scattering of $SrTiO_3$ under high pressure. High Pressure Research, 1, 53–65.

Kityk, A.V., Schranz, W., Sondergeld, P., Havlik, D., Salje, E.K.H., and Scott, J.F. (2000a) Low-frequency superelasticity and nonlinear elastic behavior of $SrTiO_3$ crystals. Physical Review B, 61, 946–956.

——— (2000b) Nonlinear elastic behaviour of $SrTiO_3$ crystals in the quantum paraelectric regime. Europhysics Letters, 50, 41–47.

Kung, J. and Rigden, S. (1999) Oxide perovskites: pressure derivatives of the bulk and shear moduli. Physics and Chemistry of Minerals, 26, 234–241.

Kung, J., Rigden, S., and Gwanmesia, G. (2000a) Elasticity of $ScAlO_3$ at high pressure. Physics of the Earth and Planetary Interiors, 118, 65–75.

Kung, J., Rigden, S.M., and Jackson, I. (2000b) Silicate perovskite analogue $ScAlO_3$: temperature dependence of elastic moduli. Physics of the Earth and Planetary Interiors, 120, 299–314.

Kung, J., Angel, R.J., and Ross, N.L. (2001) Elasticity of $CaSnO_3$ perovskite. Physics and Chemistry of Minerals, 28, 35–43.

Kung, J., Li, B., Weidner, D.J., Zhang, J., and Liebermann, R.C. (2002) Elasticity of $(Mg_{0.83},Fe_{0.17})O$ ferropericlase at high pressure: ultrasonic measurements in conjunction with X-radiation techniques. Earth and Planetary Science Letters, 203, 557–566.

Ledbetter, H., Lei, M., and Sudook, K. (1990) Elastic constants, Debye tempera-

tures, and electron-phonon parameters of superconducting cuprates and related oxides. Phase Transitions, 23, 61–70.
Lemanov, V.V. (1997) Phase transitions in $SrTiO_3$-based solid solutions. Physics of the Solid State, 39, 1468–1473.
Lemanov, V.V., Gridnev, S.A., and Ukhin, E.V. (2002) Low-frequency elastic properties, domain dynamics, and spontaneous twisting of $SrTiO_3$ near the ferroelastic phase transition. Physics of the Solid State, 44, 1156–1165.
Lheureux, D., Fischer, M., Polian, A., Itié, J.P., Gauthier, M., and Syfosse, G. (1999) Elastic properties of $SrTiO_3$ under extreme conditions: a new high pressure ultrasonic set-up. 1999 IEEE Ultrasonics Symposium, 533–536.
Li, B., Jackson, I., Gasparik, T., and Liebermann, R.C. (1996) Elastic wave velocity measurement in multi-anvil apparatus to 10 GPa using ultrasonic interferometry. Physics of the Earth and Planetary Interiors, 98, 79–91.
Li, B., Chen, K., Kung, J., Liebermann, R.C., and Weidner, D.J. (2002) Sound velocity measurement using transfer function method. Journal of Physics: Condensed Matter, 14, 11337–11342.
Li, B., Kung, J., and Liebermann, R.C. (2004) Modern techniques in measuring elasticity of Earth materials at high pressure and high temperature using ultrasonic interferometry in conjunction with synchrotron X-radiation in multi-anvil apparatus. Physics of the Earth and Planetary Interiors, 143–144, 559–574.
Liebermann, R.C. and Li, B. (1998) Elasticity at high pressures and temperatures. In R.J. Hemley and H.-K. Mao, Eds., Ultrahigh-Pressure Mineralogy, 37, p. 459–492. Reviews in Mineralogy, Mineralogical Society of America, Chantilly, Virigina.
Liebermann, R.C., Jones, L.E.A., and Ringwood, A.E. (1977) Elasticity of aluminate, titanate, stannate and germanate compounds with the perovskite structure. Physics of the Earth and Planetary Interiors, 14, 165–178.
Mishra, S.K., Ranjan, R., Pandey, D., Ranson, P., Ouillon, R., Pinan-Lucarre, J.-P., and Pruzan, P. (2005) A combined X-ray diffraction and Raman scattering study of the phase transitions in $Sr_{1-x}Ca_xTiO_3$ ($x$ = 0.04, 0.06, 0.12). Journal of Solid State Chemistry, 178, 2846–2857.
Mishra, S.K., Ranjan, R., Pandey, D., and Stokes, H.T. (2006a) Resolving the controversies about the 'nearly cubic' and other phases of $Sr_{1-x}Ca_xTiO_3$ ($0 \le x \le 1$): I. Room temperature structures. Journal of Physics: Condensed Matter, 18, 1885–1898.
Mishra, S.K., Ranjan, R., Pandey, D., Ranson, P., Ouillon, R., Pinan-Lucarre, J.-P., and Pruzan, P. (2006b) Resolving the controversies about the 'nearly cubic' and other phases of $Sr_{1-x}Ca_xTiO_3$ ($0 \le x \le 1$): II. Comparison of phase transition behaviours for $x$ = 0.40 and 0.43. Journal of Physics: Condensed Matter, 18, 1899–1912.
Niesler, H. and Jackson, I. (1989) Pressure derivatives of elastic wave velocities from ultrasonic interferometric measurements on jacketed polycrystals. Journal of the Acoustical Society of America, 86, 1573–1585.
Qin, S., Becerro, A.I., Seifert, F., Gottsmann, J., and Jiang, J. (2000) Phase transitions in $Ca_{1-x}Sr_xTiO_3$ perovskites: effects of composition and temperature. Journal of Materials Chemistry, 10, 1609–1615.
Ranjan, R., Pandey, D., Schuddinck, W., Richard, O., De Meulenaere, P., Van Landuyt, J., and Van Tendeloo, G. (2001) Evolution of crystallographic phases in $(Sr_{1-x}Ca_x)TiO_3$ with composition (x). Journal of Solid State Chemistry, 162, 20–28.
Ranson, P., Ouillon, R., Pinan-Lucarre, J.-P., Pruzan, P., Mishra, S.K., Ranjan, R., and Pandey, D. (2005) The various phases of the system $Sr_{1-x}Ca_xTiO_3$—a Raman scattering study. Journal of Raman Spectroscopy, 36, 898–911.
Ross, N.L. and Angel, R.J. (1999) Compression of $CaTiO_3$ and $CaGeO_3$ perovskites. American Mineralogist, 84, 277–281.
Salje, E.K.H., Hayward, S.A., and Lee, W.T. (2004) Ferroelastic phase transitions: structure and microstructure. Acta Crystallographica A, 61, 3–18.
Schranz, W., Sondergeld, P., Kityk, A.V., and Salje, E.K.H. (1999) Elastic properties of $SrTiO_3$ crystals at ultralow frequencies. Phase Transitions, 69, 61–76.
Sinelnikov, Y.D., Chen, G., and Liebermann, R.C. (1998a) Elasticity of $CaTiO_3$-$CaSiO_3$ perovskites. Physics and Chemistry of Minerals, 25, 515–521.
Sinelnikov, Y.D., Chen, G., Neuville, D.R., Vaughan, M.T., and Liebermann, R.C. (1998b) Ultrasonic shear wave velocities of $MgSiO_3$ perovskite at 8 GPa and 800 K and lower mantle composition. Science, 281, 677–679.
Sinelnikov, Y.D., Chen, G.L., and Liebermann, R.C. (2004) Dual mode ultrasonic interferometry in multi-anvil high pressure apparatus using single-crystal olivine as the pressure standard. High Pressure Research, 24, 183–191.
Sondergeld, P., Li, B., Schreuer, J., and Carpenter, M.A. (2006) Discontinuous evolution of single crystal elastic constants as a function of pressure through the $C2/c \leftrightarrow P2_1/c$ phase transition in spodumene, $LiAlSi_2O_6$. Journal of Geophysical Research, 111, B07202.
Webb, S., Jackson, I., and Fitz Gerald, J. (1999) Viscoelasticity of the titanate perovskites $CaTiO_3$ and $SrTiO_3$ at high temperatures. Physics of the Earth and Planetary Interiors, 115, 259–291.
Woodward, D.I., Wise, P.L., Lee, W.F., and Reaney, I.M. (2006) Space group symmetry of $(Ca_xSr_{1-x})TiO_3$ determined using electron diffraction. Journal of Physics: Condensed Matter, 18, 2401–2408.
Yamanaka, T., Hirai, N., and Komatsu, Y. (2002) Structure change of $Ca_{1-x}Sr_xTiO_3$ perovskite with composition and pressure. American Mineralogist, 87, 1183–1189.

MANUSCRIPT RECEIVED APRIL 27, 2006
MANUSCRIPT ACCEPTED SEPTEMBER 28, 2006
MANUSCRIPT HANDLED BY GEORGE LAGER